Inorganic Chemistry

Article

pubs.acs.org/IC

Aromatic Difluoroboron β-Diketonate Complexes: Effects of π-Conjugation and Media on Optical Properties

Songpan Xu, Ruffin E. Evans,‡ Tiandong Liu, Guoqing Zhang,† J. N. Demas, Carl O. Trindle, and Cassandra L. Fraser*

Department of Chemistry, University of Virginia, McCormick Road, Charlottesville, Virginia 22904, United States

Supporting Information

ABSTRACT: Aromatic difluoroboron β-diketonate complexes (BF_2bdks) are classic fluorescent molecules that have been explored as photochemical reagents, two-photon dyes, and oxygen sensors. To gain a better understanding of their emissive properties in both solution and polymer matrices, BF_2bdks with varying aromatic groups were synthesized and their photophysical properties were investigated in both methylene chloride and poly(lactic acid) (PLA). Absorption spectra showed systematic variations that are well correlated with structural features, including the size of the aryl substituent and the presence of a para electron-donating methoxy substituent. Computational modeling of the absorption spectra with the TD-B3LYP/6-311+G(d)//B3LYP/6-31G(d) formulation of density functional theory and a polarizable continuum model of dichloromethane solvent shows that all systems show intense π−π* one-electron excitations, usually from one of the highest occupied molecular orbitals (HOMO − k, k = 0, 1, 2) to the lowest unoccupied molecular orbital (LUMO). Emission properties are sensitive to the dye structure and medium. Based on spectroscopic and lifetime studies, BF_2bdks exhibit comparable fluorescence properties in both solutions and polymers when the diketonate group is functionalized with smaller aromatic ring systems such as benzene. For BF_2bdks with larger arene ring systems, such as anthracene, emission from a strong intramolecular charge-transfer (ICT) state was also noted in both solution and in PLA. There are differences in relative intensities of peaks arising from π−π* and ICT excitations depending upon dye loading in PLA. Substituent effects were also observed. Electron-donating methoxyl groups on the aromatic rings lead to enhanced fluorescence quantum yields. For certain dyes, phosphorescence is detected at low temperature or under a nitrogen atmosphere in PLA matrices.

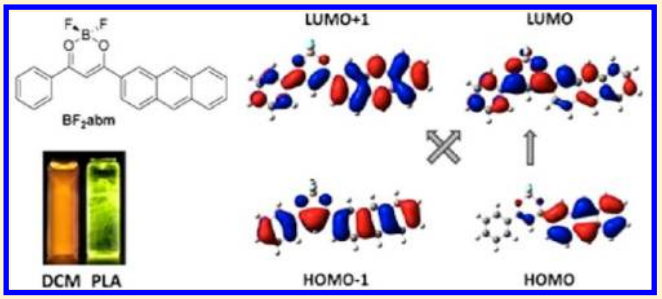

INTRODUCTION

Boron-containing materials possess impressive optical properties.[1−4] Difluoroboron β-diketonate complexes (BF_2bdks) are classic fluorescent molecules with large molar absorptivities and often high quantum yields[5] that have been explored as photochemical reagents,[6−11] two-photon materials,[12,13] conjugated polymers,[14−16] semiconductors,[17] photochromic materials,[18] near-IR probes,[19] and oxygen[20] and mechanical sensors.[21] Extensively investigated targets among these aromatic BF_2bdks are difluoroboron dibenzoylmethane (BF_2dbm) and its derivatives, given that some of the parent diketones are commercial products, such as dbm[22] and avobenzone.[23] After boronation with BF_3·OEt_2 in noncarbonyl solvents, most BF_2dbm derivatives can be obtained as air-stable, crystalline compounds. In solutions, they typically exhibit intense blue fluorescence, and some give excimer or exciplex emission[9] or dye polarity[24] effects at higher concentrations.

When BF_2dbm fluorophores are dissolved in solid-state media, such as poly(lactic acid) (PLA), also known as polylactide, long-lived room-temperature phosphorescence (RTP) is observed in the absence of oxygen.[20] Through further heavy atom perturbation, in vivo luminescence oxygen sensing and dynamic hypoxia imaging are possible in tumors,[25,26] the brain, and other contexts. BF_2dbm analogues have thus yielded promising preliminary results for cellular[27,28] and hypoxia imaging with two-photon absorbing capability and compatibility with multiphoton methods.[28] Building upon these early successes, dyes with emission profiles across the visible region are important for multiplexing, and tissue penetration depth can be increased with red-shifted dyes.[29] Although the emission wavelength of boron dye−polymer conjugate BF_2dbmPLA may be manipulated to a certain extent by polymer molecular weight, the tuning range is limited.[24] Also, this method does not shift the BF_2dbm absorption out of the UV region, which can be damaging to biological systems. Thus, the development of red-shifted BF_2bdk derivatives can expand their utility for in vitro cellular studies, ex vivo assays, and in vivo imaging agents.

Although BF_2bdk luminescence has been investigated by many groups,[5,18,30−34] ours included, we observe interesting emissive behaviors for the boron complexes in PLA compared

Received: January 12, 2012

   dx.doi.org/10.1021/ic300077g | Inorg. Chem. XXXX, XXX, XXX−XXX

to solution, which have not been reported in the literature. For example, for the naphthalene derivative, BF_2nbmPLA,[35] the fluorescence emissions in both CH_2Cl_2 and in the solid state (~440 nm) were similar to those for the benzene derivative BF_2dbmPLA under the same conditions.[20,36] However, the phosphorescence of BF_2nbmPLA showed a significant red shift (544 nm) compared to that of BF_2dbmPLA (509 nm), which suggests that π-conjugation length affects singlet and triplet states differently. Compared to the well-known difluoroboron BODIPYs (4,4-difluoro-4-bora-3a,4a-diaza-*s*-indacene),[37,38] mechanistic studies of BF_2bdk luminescence are more sparse. Therefore to better understand the optical properties of BF_2bdk complexes, including emissive states, emission color range, and media effects, it is important to conduct systematic structure–property investigations.

Here we synthesized a series of simple BF_2bdk derivatives (**1**–**10**) for a luminescence study in combination with computational chemistry. The boron complexes all possess aromatic hydrocarbons of different sizes. Compared to phenyl molecules **1**–**4**, the methoxyphenyl counterparts **5**–**8** have the same chemical structures except that the latter series has an electron-donating methoxyl group on the benzene ring to explore substituent effects. The dimethoxyphenyl BF_2bdk **9** and the methyl-naphthyl complex **10** were also included for comparison. Nomenclature for the complexes is indicated in the structures shown below. We will also refer to complexes by the hydrocarbon substituents on the difluoroboron diketonate ring [i.e., Me-Ph = mbm, **1**; Ph-Ph = dbm, **2**; Ph-Np = nbm, **3**; Ph-An = abm, **4**; Me-PhOMe = mbmOMe, **5**; Ph-PhOMe = dbmOMe, **6**; Np-PhOMe = nbmOMe, **7**; An-PhOMe = abmOMe, **8**; PhOMe–PhOMe = dbm$(OMe)_2$, **9**; Me-Np = mnm, **10**]. Fluorescence properties of these boron complexes in CH_2Cl_2 were investigated via UV–vis and fluorescence spectroscopies and quantum yield and fluorescence lifetime measurements. Computational studies were also performed to support and provide further insight into experimental findings. Also, because many useful photophysical properties of BF_2dbm derivatives arise in a solid-state environment, both fluorescence and phosphorescence were investigated for dye/PLA blends, which can inform future work with dye–polymer conjugates for imaging, sensing, and other uses.

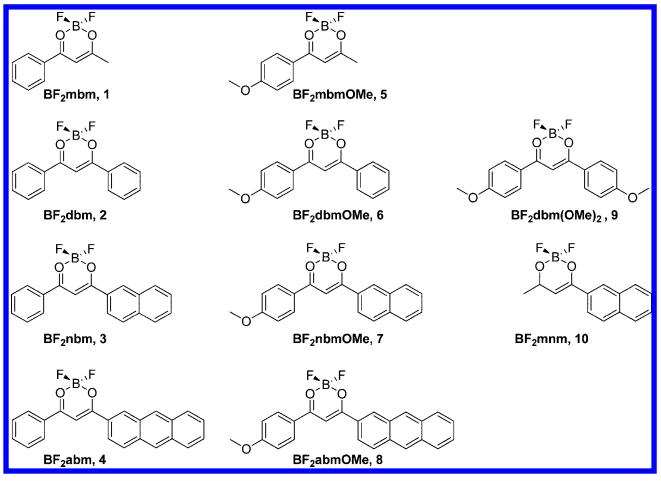

EXPERIMENTAL SECTION

Materials. Solvents CH_2Cl_2 and tetrahydrofuran (THF) were dried and purified by passage through alumina columns. Boron trifluoride diethyl etherate (Aldrich, purified, redistilled) and all other reagents and solvents were used as received without further purification. Diketone ligands were prepared by Claisen condensation with NaH, and boron complexes were prepared with BF_3 etherate as previously described. The data for complexes **1**–**4**,[39] **5**,[31] **6**,[13] **9**,[13] and **10**[31] are in accord with the literature. The synthesis of complexes **7** and **8** is described below.

Methods. ^{1}H NMR (300 MHz) spectra were recorded on a Varian UnityInova 300/51 instrument in $CDCl_3$. ^{1}H NMR spectra were referenced to the signal for residual protiochloroform at 7.26 ppm. UV–vis spectra were recorded on a Hewlett-Packard 8452A diode-array spectrophotometer. Mass spectra were recorded on an Applied Biosystems 4800 spectrometer with a matrix-assisted laser desorption ioinization tandem time-of-flight (MALDI TOF/TOF) analyzer. Elemental analysis was performed by Atlantic Microlab, Inc., Norcross, GA. Steady-state fluorescence emission spectra were recorded on a Horiba Fluorolog-3 model FL3-22 spectrofluorometer (double-grating excitation and double-grating emission monochromators). Time-correlated single-photon counting (TCSPC) fluorescence lifetime measurements were performed with a NanoLED-370 (369 nm) excitation source and DataStation Hub as the SPC controller. Lifetime data were analyzed with DataStation v2.4 software from Horiba Jobin Yvon. Fluorescence quantum yields, ϕ_F, for BF_2bdks (**1**–**10**) in CH_2Cl_2 were calculated versus anthracene in EtOH as a standard as previously described[40] using the following values: ϕ_F(anthracene) =0.27,[41] n_D^{20}(EtOH) = 1.360, and n_D^{20}(CH_2Cl_2) = 1.424. Optically dilute CH_2CH_2 solutions of BF_2bdks and EtOH solution of the anthracene standard were prepared in 1 cm path length quartz cuvettes with absorbances < 0.1. Quantum yield measurements were performed with excitation at λ_{ex} = 350 nm and emission integration range = 365–695 nm. Phosphorescence spectra were recorded with the same instrument except that a pulsed xenon lamp (λ_{ex} = 369 nm; duration <1 ms) was used for excitation and spectra were collected with a 2 ms delay after excitation. Phosphorescence lifetimes were measured with a 500 ns multichannel scaler (MCS) excited with a pulsed xenon lamp (λ_{ex} = 369 nm; duration <1 ms).

Compounds **1**–**10** were modeled with the Gaussian 09 suite of programs[42] using density functional theory for the ground-state S_0 and time-dependent density functional theory for the electronic excited states S_j, j = 1, ... The S_0 geometry optimization was conducted with B3LYP/6-31+G(d) for the ground state in vacuo and with B3LYP/6-31G(d) for the ground state in dichloromethane, modeled as a polarizable continuum according to the default method in Gaussian 09.[43,44] The optimized ground-state geometries are assured to be local minima since all computed vibrational frequencies were real. Two estimates of the triplet emission frequencies were possible; both used the optimized geometry of the lowest-energy triplet state, called T_1(opt), obtained with B3LYP/6-31G(d) in vacuo and in dichloromethane. One estimate is provided by the energy difference between T_1(opt) and the S_0 energy at the same geometry. Another estimate is obtained by TD-B3LYP/6-311+G(d) calculations of vertical S_0–T_1 electronic transitions. Both included the solvent model.[43,44] Graphic representations for self-consistent field (SCF) orbitals for the ground state were obtained with GaussView 5. Triplet structures were obtained by geometry optimization B3LYP/6-31G(d).

Difluoroboron 2-Naphthoyl-4′-methoxybenzoylmethane (BF_2nbmOMe, 7). 4-Methoxyacetophenone (150 mg, 3.0 mmol), methyl 2-naphthoate (230 mg, 1.2 mmol), and THF (20 mL) were added sequentially to a 50 mL round-bottom flask. After the mixture was stirred for 10 min, a suspension containing NaH (40 mg, 1.5 mmol) in THF (10 mL) was added dropwise at room temperature under N_2. The mixture was stirred for 20 h and then quenched with saturated aqueous $NaHCO_3$ (1 mL). THF was removed in vacuo, and then 1 M HCl (20 mL) was added. The aqueous phase was extracted with CH_2Cl_2 (3 × 20 mL), and the combined organic layers were washed with distilled water (2 × 10 mL) and brine (10 mL) and dried over Na_2SO_4 before filtration and concentration in vacuo. The residue was purified by column chromatography on silica gel eluting with hexanes/ethyl acetate (6:1) to give the diketone precursor, naphthoyl-4′-methoxybenzoylmethane (nbmOMe) as a yellow solid (240 mg,

dx.doi.org/10.1021/ic300077g | Inorg. Chem. XXXX, XXX, XXX–XXX

Table 1. Optical Properties of BF_2bdks 1−10 in CH_2Cl_2

	λ_{max},[a] nm	ε,[b] $M^{-1}\cdot cm^{-1}$	λ_{em},[c] nm	τ_F,[d] ns	ϕ_F[e]	τ_{rad}[f]	Stokes shift, cm^{-1}
1	330	31 400	416	1.04[g]	0.0031		
2	365	49 200	417	0.47	0.26	1.81	1060
	380[h]	42 900[h]	396[h]				
3	376	37 100			0.50	9.38	
	(398)[h,i]	(36300)[h]	(482)	(4.69)			(4380)
4	390	26 900	417	*j*	0.30	35	1660
	(467)[i]	(8100)	(596)	(10.5)			(4630)
5	360	39 900	393	1.02	0.65	1.57	2330
6	397	57 000	433	2.06	1.00	2.06	2090
7	415	66 300	449	1.51	0.68	2.22	1820
8	404	29 700	460[h]	1.96	0.49	21.4	2330
	(451)[i]	(11 700)	(572)	(10.5)			(4590)
9	411	73 000	437	1.79	0.78	2.29	1450
10	344	34 300			0.63	15.2	
	(380)[h,i]	(9900)	(459)	(9.55)			(4530)

[a]Absorption maxima. [b]Extinction coefficients calculated at the absorption maxima. [c]Fluorescence emission maxima. [d]Fluorescence lifetime excited with a 369 nm light-emitting diode (LED) monitored at the emission maximum. All fluorescence lifetimes are fitted with single-exponential decays unless indicated. [e]Relative quantum yield, with anthracene in EtOH as a standard. [f]Radiative lifetime, where $\tau_{rad} = \tau_F/\phi_F$. [g]Possibly multiexponential decay. [h]Band is present as a shoulder or second maximum. [i]Values in parentheses correspond to charge-transfer processes. [j]Too weak.

79%). ^{1}H NMR (300 MHz, $CDCl_3$) δ 17.10 (s, 1H, COCHCOH), 8.54 (s, 1H, 1′-ArH), 8.06−7.88 (m, 6H, 3′-, 4′-, 5′-, 8′-ArH, 3″-, 5″-ArH), 7.61−7.55 (m, 2H, 6′-, 7′-ArH), 7.03−6.99 (m, 2H, 2″-, 6″-ArH), 6.95 (s, 1H, COCHCO), 3.90 (s, 3H, -ArOMe); MS (MALDI) m/z calcd for $C_{20}H_{16}O_3$ $[M + H]^+$ 305.11, found 305.07.

Boron trifluoride diethyl etherate (81 μL, 0.64 mmol) was added to a solution of nbmOMe (130 mg, 0.43 mmol) in CH_2Cl_2 (20 mL) under N_2. The mixture was refluxed for 12 h and then the solvent was removed in vacuo. The residue was purified by column chromatography on silica gel eluting with hexanes/ethyl acetate (6:1) to give **7** as a yellow solid (123 mg, 81%). Anal. Calcd for $C_{20}H_{15}BF_2O_3$: C, 68.22; H, 4.29; F, 10.79. Found: C, 68.31; H, 4.42; F, 10.52. ^{1}H NMR (300 MHz, $CDCl_3$) δ 8.74 (s, 1H, 1′-ArH), 8.19 (d, 2H, J = 9.0 Hz, 3″-, 5″-ArH), 8.08−7.89 (m, 4H, 3′-, 4′-, 5′-, 8′-ArH), 7.66−7.60 (m, 2H, 6′-, 7′-ArH), 7.24 (s, 1H, COCHCO), 7.04 (d, 2H, J = 9.0 Hz, 2″-, 6″-ArH), 3.94 (s, 3H, -ArOMe); MS (MALDI): m/z calcd for $C_{20}H_{15}BF_2O_3Na$ $[M + Na]^+$ 375.10, found 375.03.

Difluoroboron 2-Anthracenoyl-4′-methoxybenzoylmethane (BF_2abmOMe, 8). This complex was prepared as described for **7**. Briefly, 2-acetylanthracene (101 mg, 0.45 mmol), methyl benzoate (91 mg, 0.55 mmol), and sodium hydride (46 mg, 1.82 mmol) in THF (20 mL) gave crude diketone anthroyl-4-methoxybenzoylmethane, abmOMe, which was purified by column chromatography on silica gel eluting with hexanes/ethyl acetate (6:1). The diketone was obtained as a crude yellow solid (72 mg, 45%). ^{1}H NMR (300 MHz, $CDCl_3$) δ 17.09 (s, 1H, ArCOH), 8.73 (s, 1H, 1′-ArH), 8.58 (s, 1H, 9′-ArH), 8.45 (s, 1H, 10′-ArH), 8.09−7.94 (m, 6H, 3′-, 4′-, 5′-, 8′-ArH, 3″-, 5″-ArH), 7.54−7.51 (m, 2H, 6′-, 7′-ArH), 7.03−6.96 (m, 3H, 2″-, 6″-ArH, COCHCO), 3.88 (s, 3H, -ArOMe). (A second species is suggested by minor peaks at 17.13 and 3.90 ppm.)

The boron complex was prepared via the reaction of crude abmOMe (46 mg, 0.14 mmol) and $BF_3\cdot OEt_2$ (36 μL, 0.28 mmol) in CH_2Cl_2 (20 mL) and was purified via column chromatography on silica gel eluting with hexanes/ethyl acetate (1:1) to give **8** (30 mg, 57%) as a red solid. Anal. Calcd for $C_{24}H_{17}BF_2O_3$: C, 71.67; H, 4.26; F, 9.45. Found: C, 71.50; H, 4.20; F, 9.25. ^{1}H NMR (300 MHz, DMSO-d_6) δ 9.30 (s, 1H, 1′-ArH), 8.91 (s, 1H, 9′-ArH), 8.70 (s, 1H, 10′-ArH), 8.44 (d, 2H, J = 8.7 Hz, 3″-, 5″-ArH), 8.27−8.14 (m, 4H, 3′-, 4′-, 5′-, 8′-ArH), 8.01 (s, 1H, COCHCO), 7.67−7.58 (m, 2H, 6′-, 7′-ArH), 7.23 (d, 2H, J = 8.7 Hz, 2″-, 6″-ArH), 3.94 (s, 3H, -ArOMe); MS (MALDI) m/z calcd for $C_{24}H_{17}BF_2O_3Na$ $[M + Na]^+$ 425.11, found 425.13.

RESULTS AND DISCUSSION

The boron complexes were synthesized by Claisen condensation with NaH to generate the β-diketones, followed by boronation with $BF_2\cdot OEt_2$ in CH_2Cl_2. The rate of Claisen condensation drops and the product solubility decreases with increasing arene size. All of the complexes were obtained as yellow crystals except for the anthryl compounds **4** and **8**, which are dark red powders. The synthesis and solid-state fluorescence and mechanochromic properties for compounds **1**−**4** have been described elsewhere.[39]

Absorption Spectra in CH_2Cl_2. The optical properties of compounds **1**−**10** (Table 1) were first studied in CH_2Cl_2 because these conditions do not result in boron−ligand dissociation,[45] exciplex formation,[46,47] or photochemical reactions[7,8] seen for solvents containing Lewis bases, aromatic rings, or double bonds. Absorption spectra show that all ten complexes have high extinction coefficients (26 900−73 000 $M^{-1}\cdot cm^{-1}$), which is typical of $\pi-\pi^*$ transitions (Figure 1). Complex **9** with two methoxyl benzene rings has the strongest absorption, whereas the weakest absorptions occur for complexes containing the anthracene moiety, namely, **4** and **8**. Compared with complexes **1**−**4**, complexes **5**−**8** show similar but stronger and red-shifted absorption spectra, since the methoxyl substituent possesses electron-donating ability. Another difference between the two sets of compounds is that **5**−**8** exhibit slightly sharper absorption spectra [i.e., smaller full width at half-maximum (fwhm) for major absorption bands], perhaps due to more rigid structures from the electron-donating methoxyl groups (inferred from resonance structures). Figure 1C compares BF_2dbm (**2**) with mono- (**6**) and dimethoxy-substituted (**9**) derivatives to explore substituent effects. As for **5**−**8**, in this series too, increasing donor strength correlates with stronger absorption and red-shifted emission. The naphthylmethyl complex **10** is included because **2** and **10** have similar π conjugation lengths; however, the absorption of **10** is different from **2** in two aspects. First, **10** shows a bimodal absorption spectrum (344 and ∼380 nm shoulder), as is also noted for complexes **4** (390 and 467 nm) and **8** (404 and 451 nm); second, the absorption maximum of **10** is far more blue-shifted than the rest. From the absorption spectra in CH_2Cl_2, it

dx.doi.org/10.1021/ic300077g | Inorg. Chem. XXXX, XXX, XXX−XXX

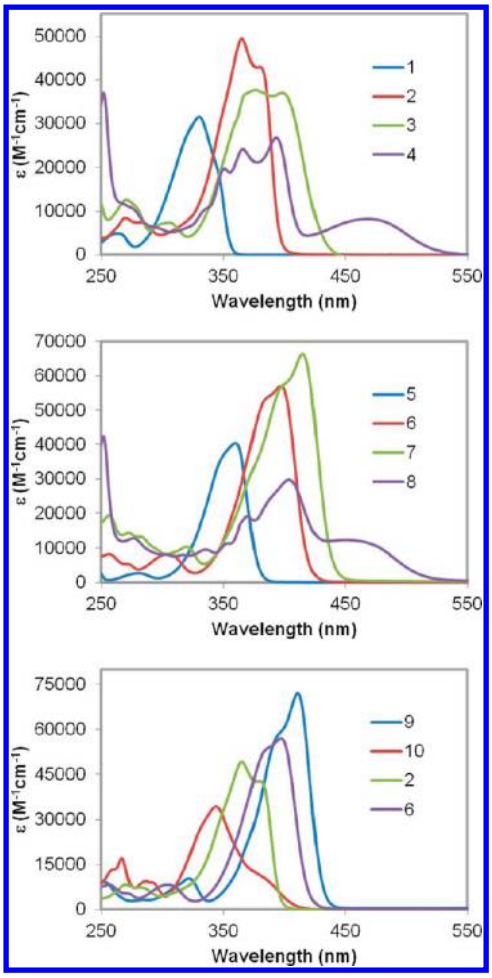

Figure 1. Absorption spectra of BF_2bdk complexes **1**−**10** in CH_2Cl_2.

is reasonable to believe that complexes **4**, **8**, and **10** (which also have the smallest extinction coefficient values) have significant intramolecular charge-transfer (ICT) character compared to the rest, as evidenced by a second structureless, red-shifted absorption band in addition to the main absorption peak. One common feature shared by the three molecules (**4**, **8**, and **10**) is that they are the most unsymmetrically substituted in terms of arene sizes on the diketonate. More definitive conclusions may be reached after the emission spectral analysis and computational results are presented below.

Fluorescence in CH_2Cl_2. Emission spectra and fluorescence lifetimes of the complexes were also measured. The results are given in Figure 2 and Table 1. As shown in the photograph in Figure 2, under UV illumination, all the complexes exhibit intense fluorescence ranging from violet to orange-red except for **1**, which only faintly fluoresces in the violet-blue region. The Stokes shift, the difference in energy between the emission-state energy and the energy of its emitting-state absorption, is also included. In several cases the lowest energy absorption or highest energy emission bands were estimated from a shoulder or a weaker peak than the absolute maximum (see Table 1, footnote *h*). For the dual-emitting complexes **4** and **8**, data are reported for both emissions from each complex. The complexes are grouped into two categories. One has large Stokes shifts (~4500 cm^{-1}) with long radiative lifetimes (>9 ns); these include **3**, **10**, and the low-energy emissions of **4** and **8**. The other complexes and the

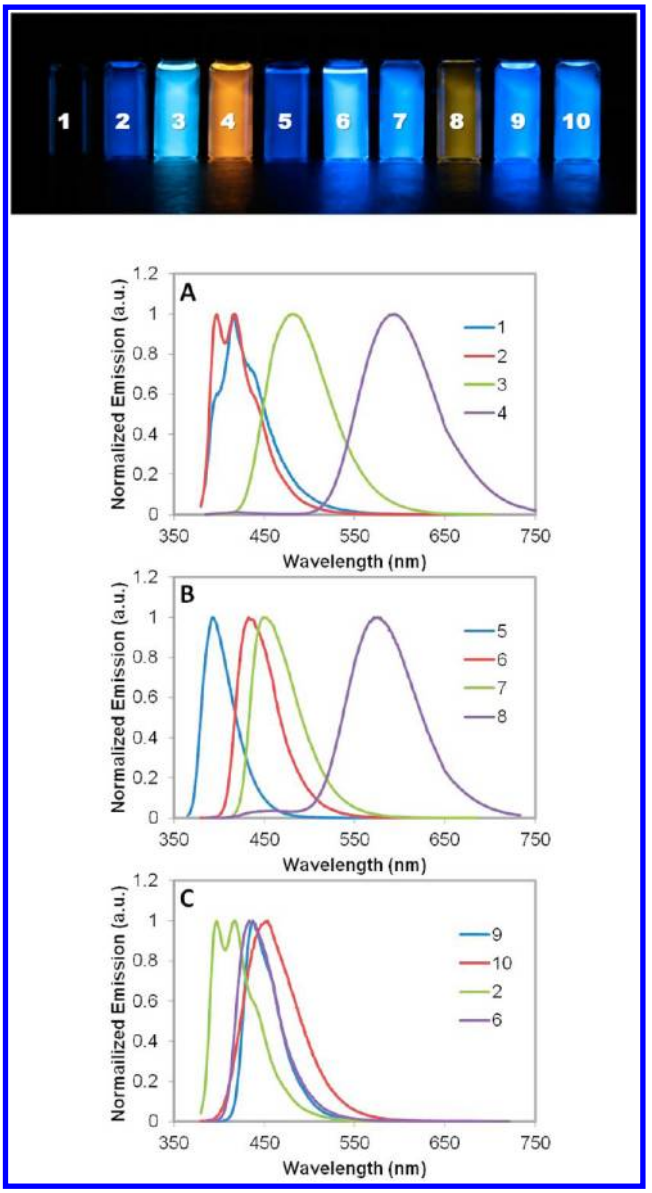

Figure 2. Photographs and steady-state emission spectra of BF_2bdks **1**−**10** in CH_2Cl_2 (λ_{ex} = 369 nm).

high-energy emissions of **4** and **8** have small Stokes shifts (1200−2500 cm^{-1}) and short radiative lifetimes (2 ns). As will be shown, these emissions arise from different types of excited states.

Theoretically, an increase in π conjugation length typically brings about a red shift of emission and change in quantum yield.[48] The spectra roughly follow this rule but exceptions were also observed. For example, the π-donating methoxyl substituent extends the conjugation of **8** through π donation compared to **4**; however the emissions of **8** are blue-shifted compared with **4**. The same trend was observed for the naphthalene-containing BF_2bdks **3** (Ph-Np, 482 nm), **7** (Np-PhOMe, 449 nm), and **10** (Me-Np, 459 nm), where the greatest π conjugation (**7**) results in the most blue-shifted emission in CH_2Cl_2. This observation indicates that conjugation length is not the only parameter that influences the emissive state energy of the complexes. This signals that other factors such as inductive effects or charge transfer are involved, as we will discuss in greater detail below.

dx.doi.org/10.1021/ic300077g | *Inorg. Chem.* XXXX, XXX, XXX−XXX

The fluorescence lifetimes of the complexes were also measured and the results are collected in Table 1. The radiative lifetime for each molecule is given by

$$\tau_{rad} = \tau_F/\phi_F \quad (1)$$

where τ_F and ϕ_F are the observed lifetime and luminescence quantum yield, respectively. This value, τ_{rad}, which is also known as the instrinsic lifetime, is the lifetime that would be measured if the there were no radiationless processes competing with the luminescence decay. The radiative lifetime τ_{rad} is a direct measure of the allowedness of the emission. Optically dilute complexes **2**−**10** exhibited single-exponential decays in CH_2Cl_2. The decay of **1** was very weak ($\phi_F < 0.004$) with an estimated multiexponential lifetime of ∼1 ns. Given the weak emission, the absence of a mirror-image relationship between the absorption and emission, and the anomalously long lifetime for the low quantum yield, we attribute the emission to trace impurities, possibly a very low concentration conformer, given that it persists from preparation to preparation, and we consider **1** to be nonluminescent or extremely weakly luminescent. The anthracene-containing complexes **4** (Ph-An) and **8** (An-PhOMe) displayed especially long fluorescence decay (10.5 ns), whereas BF_2dbm exhibited the shortest decay (0.47 ns) despite its reasonably large fluorescence quantum yield ($\phi_F = 0.26$). However, the addition of one (**6**) or two (**9**) methoxy groups onto BF_2dbm increases the quantum yields of **6** and **9** considerably.

An interesting result was also observed for the fluorescence lifetimes of the most unsymmetric molecules. Complexes **3**, **4**, **8**, and **10**, with different diketonate arenes (or Me), have the longest radiative decay times (**3**, nbm, τ_{rad} = 9.38 ns; **4**, Ph-An, τ_{rad} = 35.0 ns; **8**, An-PhOMe, τ_{rad} = 21.4 ns; and **10**, Me-Np, τ_{rad} = 15.2 ns). The remaining complexes, including symmetrically substituted complexes such as **2** (Ph-Ph) and **9** (PhOMe−PhOMe), all have much shorter radiative decays of about 2 ns. The differences in lifetimes for **3**, **4**, **8**, and **10** coupled with the presence of weaker long-wavelength absorption bands for **4**, **8**, and **10** indicate a fundamentally different type of excited-state emission. Though not as distinct in the UV−vis spectrum for **3**, it could still be argued that the low-energy feature evident at ∼400 nm on the absorbance band also arises from (albeit weaker) ICT. This is also supported by computational results presented below.

As stated above, distinct low-intensity red features in the absorption spectra for unsymmetrical complexes **4**, **8**, and **10** are ascribed to intramolecular charge transfer, ICT. Computational modeling discussed below supports this assertion; these features are dominated by excitations in which charge is transferred from the larger, more electron-rich arene toward the boron diketonate center. The second and more intense feature lying at higher energy is a $\pi-\pi^*$ transition where both π and π^* are delocalized throughout the molecule. Since both molecular orbitals (MOs) occupy a common space, the transition has little ICT character. In the other more symmetric structures such as **2** or **9**, the $\pi-\pi^*$ transition is at lower energy than any ICT transition and dominates the long-wavelength region of the absorption spectrum. As a result, shorter radiative decay lifetimes are expected.

These observations about absorbance also inform the interpretation of Ph-An (**4**) and An-PhOMe (**8**) complex emissions, where **4** has a stronger ICT tendency than **8**. From the fluorescence spectra, the emission maximum of **4** is red-shifted by 24 nm (704 cm^{-1}) compared to that of **8**. Though the π-donating methoxy group does not seem to make a difference in terms of the fluorescence decay (τ_F = 10.5 ns for both **4** and **8**), the radiative lifetimes follow the expected trend, given the differing quantum yields. For **4**, τ_{rad} is nearly double the value for **8**, indicating a large long-lived contribution from the ICT state. ICT from anthracene to the diketonate group is significant regardless of whether benzene or methoxybenzene is present as a competing donor group. In this process, the phenyl ring may serve largely as a substituent on the acceptor. The more electron-rich MeO-Ph ring (versus Ph) may slightly weaken the acceptor ability of the boron diketonate ring, thus increasing the energy of the transition. In comparison to anthracene dyes **4** and **8**, the phenyl derivatives **2** (Ph-Ph, τ_{rad} = 1.81 ns), **9** (PhOMe−PhOMe, τ_{rad} = 2.29 ns), and **6** (Ph-PhOMe, τ_{rad} = 2.06 ns) are symmetrically substituted molecules with respect to the arenes and they show relatively short fluorescence decay. Within this series, where $\pi-\pi^*$ transitions likely dominate the electronic transitions, the methoxy substituents exert a subtle but measurable effect on fluorescence decay.

Complexes **4** and **8** exhibit dual emissions (Table 1). There is a weak high-energy emission and stronger low-energy emission. The two emissions in spectra for species **4** and **8** clearly derive from distinct ground state species given different excitation spectra, provided in the Supporting Information. Both low- and high-energy emissions for **8** have a single-exponential decay (Table 1). The same is true for **4**, though the high-energy emission is weak; a lifetime could not be obtained. Furthermore, there is no negative preexponential factor for the long-lived emission in either case, which establishes that the low-energy emissions are not arising from the state responsible for the high-energy emission. We suggest that there are two ground-state conformers for these complexes. One has a structure conducive to the $\pi-\pi^*$ state being lowest energy in the excited state and gives rise to a short-lived (∼2 ns) $\pi-\pi^*$ fluorescence. The dominant structure gives an ICT excited state lowest in energy and is the source of the much longer-lived ICT emission (10.5 ns).

In summary, absorption and fluorescence data indicate moderate to strong ICT character for unsymmetrically substituted difluoroboron diketonates **3**, **4**, **8**, and **10**, while $\pi-\pi^*$ transitions dominate for symmetrically substituted compounds (e.g., **2** and **9**). This is consistent with known solvatochromic properties of this family of dyes, as charge-separated states are sensitive to the polarity of the surrounding medium.[13,49] The electronic transitions of the BF_2bdks depend on their molecular symmetries. A greater disparity in π-electron-donating ability of the two arene rings seems to result in a stronger ICT state dominated by the more electron-rich aryl group. When the bdk arene ring sizes are comparable, in more symmetrical structures, a delocalized $\pi-\pi^*$ model is proposed. These experimental conclusions are supported by computational studies discussed below.

Computational Studies. The Gaussian 09 software suite[42] was used for all computational modeling. Optimized geometries for species **1**−**10** were determined with a density functional theory (DFT) method, B3LYP/6-31G(d). The absorption spectra were characterized by time-dependent (TD) density functional theory, specifically TD-B3LYP, in a more flexible basis, 6-311+G(d). TD-DFT methods represent excited states as combinations of the single excitations of an electron from an orbital occupied in the SCF ground state to an orbital in the set vacant in the ground state. The wavelength and intensity of

dx.doi.org/10.1021/ic300077g | Inorg. Chem. XXXX, XXX, XXX−XXX

vertical absorption transitions correlate well with experimental counterparts, with R^2 = 0.91 between absorption wavelengths computed with no consideration of solvent effects and the band maxima as reported in Table 1. Incorporation of solvent effects by the polarizable continuum model (Tomasi's PCM) brings predicted absorption wavelengths into close agreement with observed values, increases R^2 to 0.96, and also slightly improves the estimates of absorption intensities. The calculations, in vacuo or with solvent treatment, not only capture the general form of the absorption curves but also track the intensity enhancement and wavelength shifts attending structural changes. The Supporting Information contains graphs of computed spectra and pictures of relevant orbitals, which may aid in comparison.

Trends in the computed and observed absorption spectra can be described most easily by considering subsets of related molecules. The family **1**−**4** has a common Ph-R structure and dye group **5**−**8** has a common structure of PhOMe-R, with R = methyl, phenyl, naphthyl, and anthryl. The subset **1**, **5**, and **10** (Me-Ph, Me-PhOMe, and Me-Np respectively) allows examination of the relative effects of methoxy substitution and extending the aryl from phenyl to naphthyl. Finally the subset **2**, **6**, and **9** (Ph-Ph, Ph-PhOMe, and PhOMe−PhOMe, respectively) allows discussion of the cumulative effects of methoxy substitution.

The families **1**−**4** and **5**−**8** show a red shift in the low-energy edge of the optical spectrum as the aryl substituent increases in size. Extending the size of the arene raises the energy of its highest occupied molecular orbital (HOMO). If there is a reasonable energy match between the HOMO for the aryl fragment and MOs in the boron-containing ring, there will be substantial mixing between them. This gives rise to delocalization over the entire molecule, elevation of the highest occupied MO, and a redder transition. If the energy match is poor, the aryl MO remains localized, and the HOMO (aryl) to lowest unoccupied molecular orbital (LUMO) (delocalized) transition changes character to a charge transfer. The charge-transfer band may have relatively weak intensity, owing to reduction in Franck−Condon factors, and can be very red. It has been noted that most DFT functionals, including B3LYP, is generally inaccurate in predicting transition energies involving long-range ICT states.[50,51] Nonetheless, this feature of the absorption spectra is captured by the modeling, and is a significant part of what we see in the anthryl-substituted species **4** and **8**, where contrast between aryl rings is greatest and the effect on the spectrum is most pronounced. Similar but less evident features are found for **3** and **10**. For example, the computed spectrum for complex **3** suggests the presence of a weak absorption with some ICT character, to the red of a stronger $\pi-\pi^*$ transition. The weaker red absorption computed at 430 nm may not be clearly distinguishable from the stronger blue transition computed at 372 nm owing to the breadth of the absorption bands. As inferred from the experimental observations, compound **4** appears to have the greatest ICT character. See Figure 3 for a visualization of transitions for molecules **2** and **4** determined with the solvent correction. Table 2 contains a more detailed summary of these results.

It is interesting to note that species **4** and **8** display the strongest Stokes shift in the emission. That is in accord with with the substantial geometrical rearrangement to be expected in the charge-transfer excited state. It is clear that the modeling is entirely consistent with the interpretation of the experimental absorption spectra and lends indirect support to the ideas

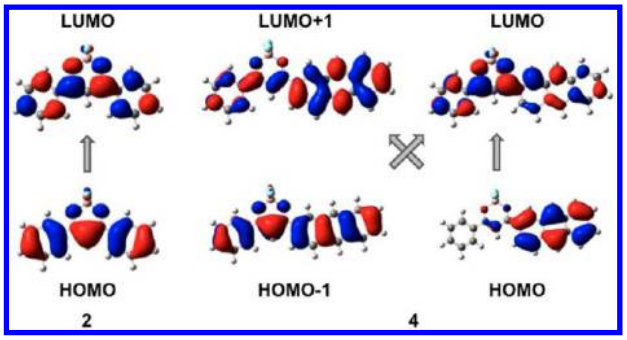

Figure 3. Orbitals involved in the absorption spectra for complexes **2** (Ph-Ph) and **4** (Ph-An) in methylene chloride medium.

expressed in the discussion of the emission properties of these systems.

When aryl substituents on the difluoroboron diketonate ring are identical (**2**), spectra are dominated by HOMO to LUMO excitations; both orbitals are delocalized throughout the molecule. When the substituents are very different (**4**), the spectrum has a broad weak red feature, derived from a HOMO − LUMO ICT transition, and a higher-energy more intense feature, in which the HOMO − 1 to LUMO and HOMO to LUMO + 1 excitations are strongly mixed. Additional orbital depictions and characterization of the transitions may be found in the Supporting Information.

Modeling permits further remarks on the absorption spectra. In most cases one can discern two strongly overlapping bands in the leading red edge of the optical absorption spectra. The two bands seem to grow more separate and distinct as the size of the aromatic substituent grows, in either series **1**−**4** or **5**−**8**, until they become entirely separate in **4** and **8**. This is evidently another consequence of the systematic elevation of the highest occupied MO of the aryl moiety, which eventually allows distinct $\pi-\pi^*$ transitions: first the low-energy ICT from HOMO to LUMO and then the fully delocalized HOMO − 1 to LUMO.

The spectra for subset **1**, **5**, and **10** (Me-Ph, Me-PhOMe, and Me-Np, respectively) suggest that methoxy substitution on phenyl elevates the highest occupied MO without blocking its delocalization, while extending the aryl to naphthyl localizes the highest occupied MO more thoroughly on the aryl fragment. In the computed spectrum a weak red HOMO to LUMO transition distinct from the more intense and higher energy HOMO − 1 to LUMO feature is noted. This finds its counterpart as a red shoulder in the first broad absorption band of the experimental spectrum.

Finally the sequence of methoxy substitution in subset **2**, **6**, and **9** (Ph-Ph, Ph-PhOMe, and PhOMe−PhOMe, respectively) shows successive red shifts and intensity enhancements as first one and then two *p*-methoxy substituents are introduced. Each methoxy elevates its aryl highest occupied MO without going so far as to impede delocalization. Again, computed results correlate with experiment.

Even approximate treatment of solvent effects has had some positive effects. For example, the excitation wavelength calculated in vacuo is always blue-shifted compared to the experimental value; the PCM version of the polar solvent dichloromethane induces a red shift, toward the experimental values. This behavior is consistent with the observed solvatochromism of this class of compounds.[13,49] The calculation is still approximate however, and absorption

dx.doi.org/10.1021/ic300077g | *Inorg. Chem.* XXXX, XXX, XXX−XXX

Table 2. Comparison of Experimental and Calculated Optical Properties of BF_2bdks 1−10 in CH_2Cl_2 and in Vacuo

	λ_{max},[a] nm	ε,[b] $M^{-1}\cdot cm^{-1}$	λ_{calc} CH_2Cl_2,[c] nm	f[d]	λ_{calc} in vacuo,[e] nm	f[f]	transition type
1	330	31 400	306	0.6111	306	0.4671	$\pi-\pi^*$
2	365	49 200	364	0.9764	342	0.7761	$\pi-\pi^*$
3	376	37 100	372	0.9648	353	0.8200	$\pi-\pi^*$
	398[g]	36 300[g]	430	0.2791			ICT
4	390	26 900	385	0.8325	359	0.9262	$\pi-\pi^*$
	467	8100	539	0.2525	498	0.1723	ICT
5	360	39 900	338	0.8090	325	0.7202	$\pi-\pi^*$
6	397	57 000	387	1.0768	361	0.8994	$\pi-\pi^*$
7	415	66 300	389[h,i]	0.7417	367	0.7811	$\pi-\pi^*$
			422[h,i]	0.6436			
8	404	29 700	403	1.2386	382	0.7828	$\pi-\pi^*$
	451	11 700	525	0.3155	485	0.2092	ICT
9	411	73 000	399	1.2893	370	1.1035	$\pi-\pi^*$
10	344	34 300	338	0.7263	324	0.5522	$\pi-\pi^*$
	380[g]	9900	405	0.1541	380	0.106	ICT

[a]Experimental absorption maxima in dichloromethane. [b]Extinction coefficients calculated at the absorption maxima in dichloromethane. [c]Computed transition wavelength (in dichloromethane medium). [d]Computed oscillator strength (in dichloromethane medium). [e]Computed transition wavelength (in vacuo). [f]Computed oscillator strength (in vacuo). [g]Low-energy ICT band is present as a shoulder. [h]Two overlapping transitions: ε is proportional to the sum of squares of f's. [i]Complex **7** exhibits two transitions of roughly comparable energy. These each have some ICT character but are predominantly $\pi-\pi^*$.

intensities are poorly described. In particular, compounds **4** and **8** have much weaker absorption than their relatively high oscillator strengths would predict. It may be that more advanced methods[52,53] can be employed to better estimate the excitation energies of this family of complexes.

Polymer Medium Effects: Fluorescence of BF_2bdk/PLA Blends. The optical properties of the BF_2bdk series were also measured in poly(lactic acid), a solid-state solvent, at both room temperature and 77 K with two different dye loadings. The PLA used in the experiment was synthesized via solvent-free ring-opening polymerization.[54] Boron complexes **1**−**10** and PLA were dissolved in CH_2Cl_2 to form a homogeneous solution that was used to cast a thin film onto the inner wall of a small vial. The film was then thoroughly dried in vacuo before luminescence measurements. The measured optical properties for these blends at room temperature are presented in Figure 4 and Table 3.

Compared to the emission data in CH_2Cl_2, for the more dilute 0.05% (w/w) dye/polymer loading, the fluorescence emission maxima at room temperature are typically blue-shifted in the PLA substrate, possibly because PLA is a less polar and more rigid medium than CH_2Cl_2. A combination of solvatochromic and rigidochromic effects[55] may explain the blue shifts, which are greatest for emissions associated with ICT transitions of complexes **4** (Ph-An) and **8** (An-PhOMe) (64 and 58 nm, i.e., 2018 and 1972 cm^{-1} respectively) with large anthracene substituents. This too supports the hypothesis that the strongest ICT states are present in these anthracene complexes, because in the solid-state solvent PLA, the presumed ICT "twisted configuration" may be hindered.[56] The emission spectra from **4** and **8** in PLA are bimodal, with **4** possessing a more conspicuous high-energy shoulder at 419 nm and **8** at 430 nm). In fact, even in CH_2Cl_2, both **4** and **8** have additional high-energy bands around 417 and 460 nm, respectively (Figure 2), which are weaker compared to those recorded in PLA. It is not uncommon to observe dual emission bands for donor−acceptor fluorescent molecules in polar solvents. According to twisted intermolecular charge-transfer (TICT) theory,[29] the two distinct fluorescence emission bands of complexes **4** and **8** might be ascribed to a TICT state (lower energy) and a coplanar locally excited state (higher energy), as discussed above for solution and computational studies. Interestingly, the shoulder emission of complex **4** shares almost the same emission maxima and vibronic features as those for the dbm complex **2**; similarly for complex **8**, the higher energy shoulder closely matches to the fluorescence of dbmOMe complex **6**.

The fluorescence lifetimes measured for the complexes in PLA were all fitted to triple-exponential decays, except for the Me-Ph derivative **1**, which did not show strong enough intensity for measurement with the current instrument setup. As has been described previously, the solid-state polymeric environments are heterogeneous, and therefore multiexponential decays are common for BF_2bdks.[20] Compared to fluorescence lifetimes recorded in CH_2Cl_2, the values obtained in PLA did not follow an obvious trend. However, we did observe some reductions in τ_F in PLA versus CH_2Cl_2 for molecules that exhibited strong ICT character (e.g., ICT band in PLA vs CH_2Cl_2: **4**, 10.1 vs 10.5 ns; **8**, 9.12 vs 10.5 ns; and **10**, 5.35 vs 9.55 ns), which again suggests that the ring twisting may be partially inhibited or that there are reduced relaxation effects in the rigid and less polar PLA matrix at room temperature.

From the steady-state fluorescence spectra, most of the polymer films with higher dye loading exhibit slightly red-shifted emission maxima (Table 3 and Figure 4), likely due to the exciton coupling or "fluorophore−fluorophore interaction"[24] as previously reported. Methyl dyes **1** and **10** lacking a methoxyl substituent and the dbm complex **2** serve as exceptions. The fluorescence lifetimes, accordingly, are consistently longer for molecules showing red-shifted emission maxima at higher concentrations. The increase in lifetimes for high dye loadings has also been discussed in terms of dye−dye interactions, where excimeric species are likely to form. The propensity of BF_2bdk dyes to form H aggregates has also been advanced as a possibility.[57]

Temperature effects were also studied by collecting steady-state emission spectra at 77 K in liquid nitrogen for all BF_2bdk/PLA blends at two different dye loadings (Figure 5 and Table

dx.doi.org/10.1021/ic300077g | Inorg. Chem. XXXX, XXX, XXX−XXX

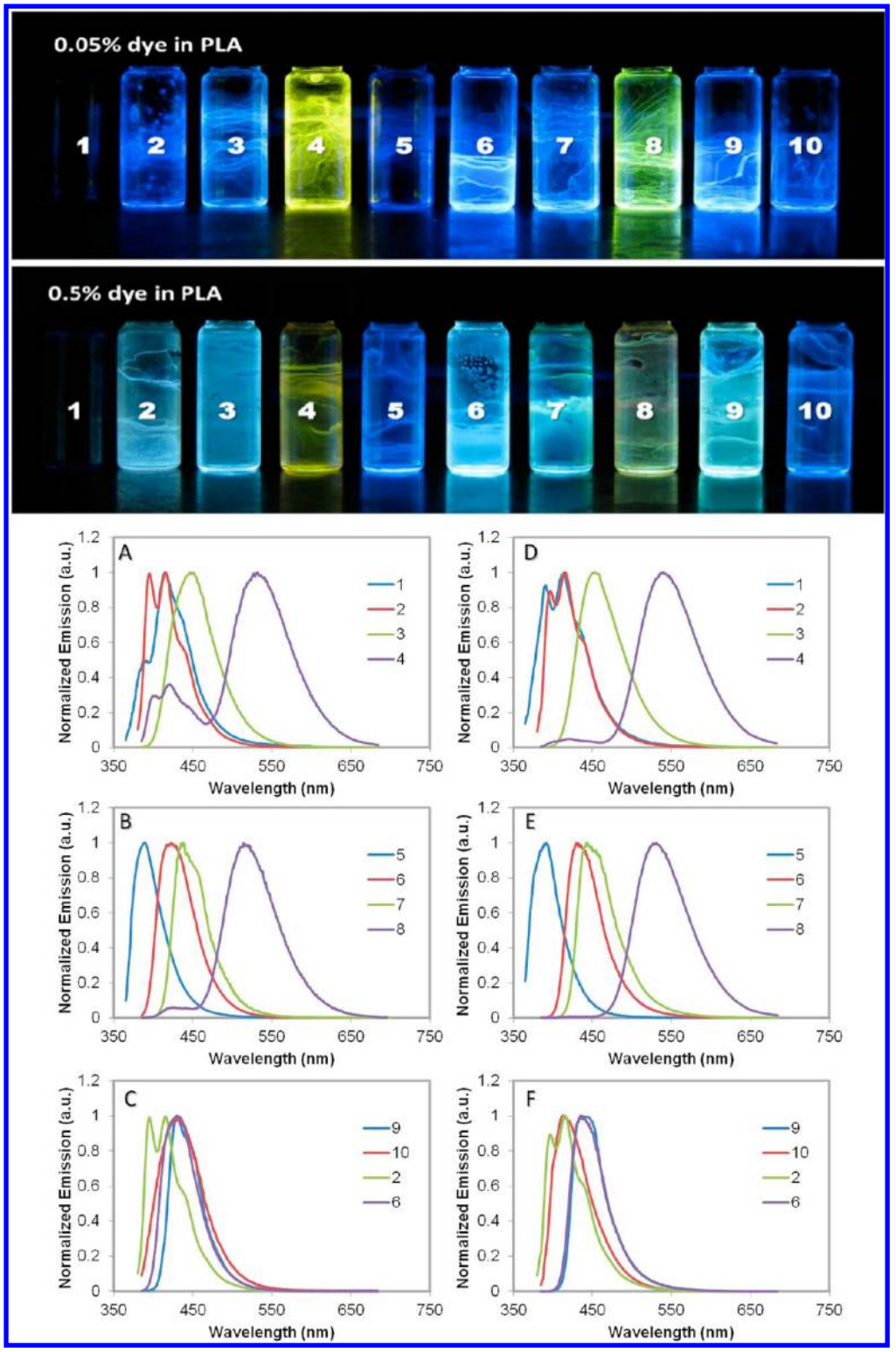

Figure 4. Photograph and steady-state emission spectra of BF_2bdk/PLA blends at (A–C) 0.05% and (D–F) 0.5% dye loadings at room temperature. (λ_{ex} = 369 nm except for **1** and **5**, where λ_{ex} = 350 nm).

4). For dye blends at lower concentrations, most emission maxima are slightly blue-shifted, probably due to the rigidochromic effect at liquid nitrogen temperature. The blue shifts are generally small; the low loading of compound **2** is even slightly red-shifted, indicating that PLA at room temperature, below the glass transition temperature of ~60 °C, is already rather rigid. At low temperature, the emission spectra also show sharper vibrational structure for complexes **1**–**4**. The spectra are also narrowed for BF_2bdks **5**–**8**, which have methoxy substitutions, and exhibit less prominent vibrational features. Furthermore, distinct phosphorescence bands are observed for certain complexes at low temperature (e.g., naphthyl complexes **3**, 537 nm; **7**, 538 nm; and **10**, 523 nm). Further discussion of the emissive triplet state for these materials is provided below.

dx.doi.org/10.1021/ic300077g | *Inorg. Chem.* XXXX, XXX, XXX–XXX

Table 3. Optical Properties of BF_2bdk/PLA Blends at Room Temperature

	0.05% (w/w) BF_2bdk/PLA		0.5% (w/w) BF_2bdk/PLA	
	λ_F,[a] nm	τ_F,[b] ns	λ_F,[a] nm	τ_F,[b] ns
1	415	*c*	413	*c*
2	415	1.82	415	1.67
3	448	2.31	453	3.66
4	419	*d*	428	1.81
4[e]	(532)	(10.1)	(540)	(10.8)
5	389	0.61	392	0.89
6	427	2.36	435	3.79
7	437	1.44	443	1.83
8	430	1.22	430	1.98
8[e]	(514)	(9.12)	(531)	(13.43)
9	429	2.44	435	3.71
10	429	5.35	413	6.58

[a]λ_{ex} = 369 nm. [b]Pre-exponential weighted lifetimes. All fluorescence lifetimes were fitted with triple-exponential decays. [c]Signal too weak to be detected with current LED excitation. [d]Weak. [e]Values in parentheses correspond to charge-transfer processes.

Table 4. Optical Properties of BF_2bdk/PLA Blends at 0.05% and 0.5% Dye Loadings at 77 K

	0.05% (w/w) BF_2bdk/PLA		0.5% (w/w) BF_2bdk/PLA	
	λ_F,[a] nm	τ_F,[b] ns	λ_F,[a] nm	τ_F,[b] ns
1	412[c]	*d*	391[c]	*d*
2	421	2.11	413[c]	2.19
3	441	2.40	449	3.33
4	418	*e*	418	1.54
4[f]	(524)	(9.35)	(531)	(10.10)
5	385	0.64	387	0.84
6	422	2.06	435	2.12
7	434	1.42	425	1.39
8	427	1.85	431	2.03
8[f]	(523)	(7.87)	(529)	(8.31)
9	425	1.77	432	1.75
10	426	6.59	409[c]	7.81

[a]Excited with 369 nm LED. [b]Pre-exponential weighted lifetimes. All fluorescence lifetimes were fitted with triple-exponential decays. [c]Excited at 350 nm. [d]Signal too weak to be detected with current LED excitation. [e]Weak. [f]Values in parentheses correspond to charge-transfer processes.

Low-temperature fluorescence lifetimes were also examined for comparison with room-temperature data. Most compounds have moderately increased fluorescence lifetimes, as expected at lower temperatures due to less collisional quenching. However, more significant differences in both emission spectra and lifetimes were observed for the 0.5% dye/PLA blends at 77 K. Many of the differences are probably caused by inhibition of excimer formation at liquid nitrogen temperature and a significant reduction in fluorescence lifetimes (e.g., lifetime

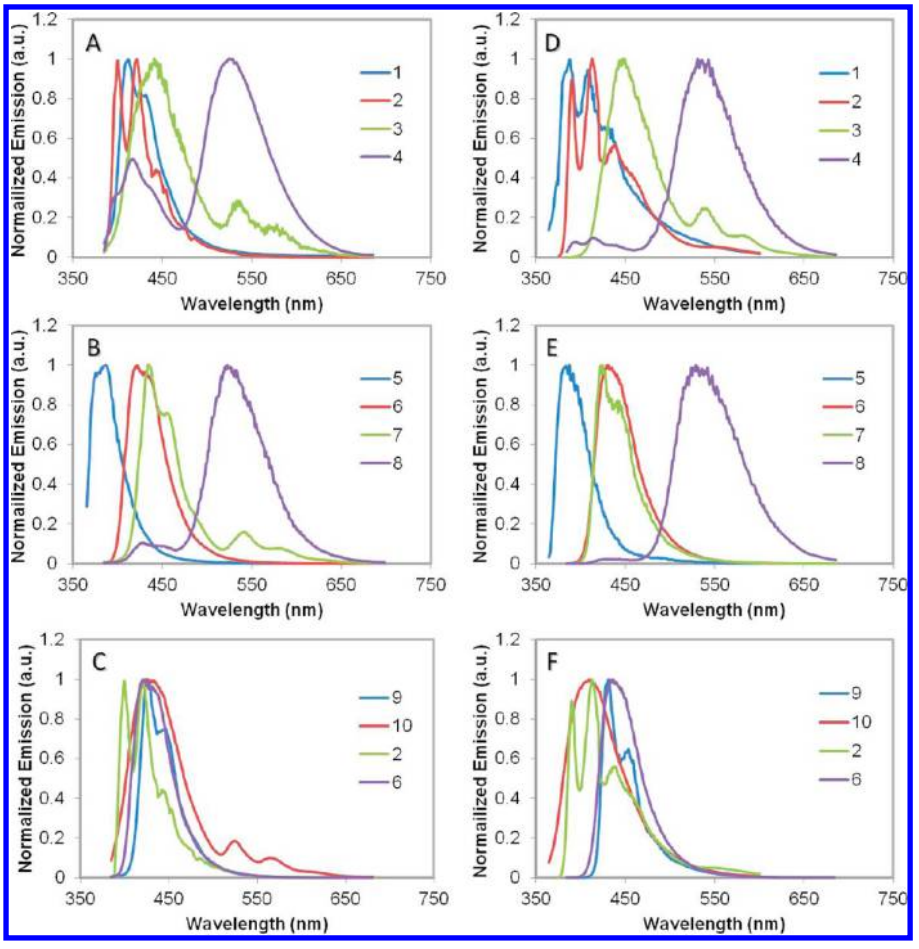

Figure 5. Fluorescence emission of BF_2bdk/PLA blends at (A–C) 0.05% and (D–F) 0.5% dye loading at 77 K (λ_{ex} = 369 nm except for **1** and **2** at 0.5% loading and **5** for both loadings, where λ_{ex} = 350 nm).

dx.doi.org/10.1021/ic300077g | *Inorg. Chem.* XXXX, XXX, XXX–XXX

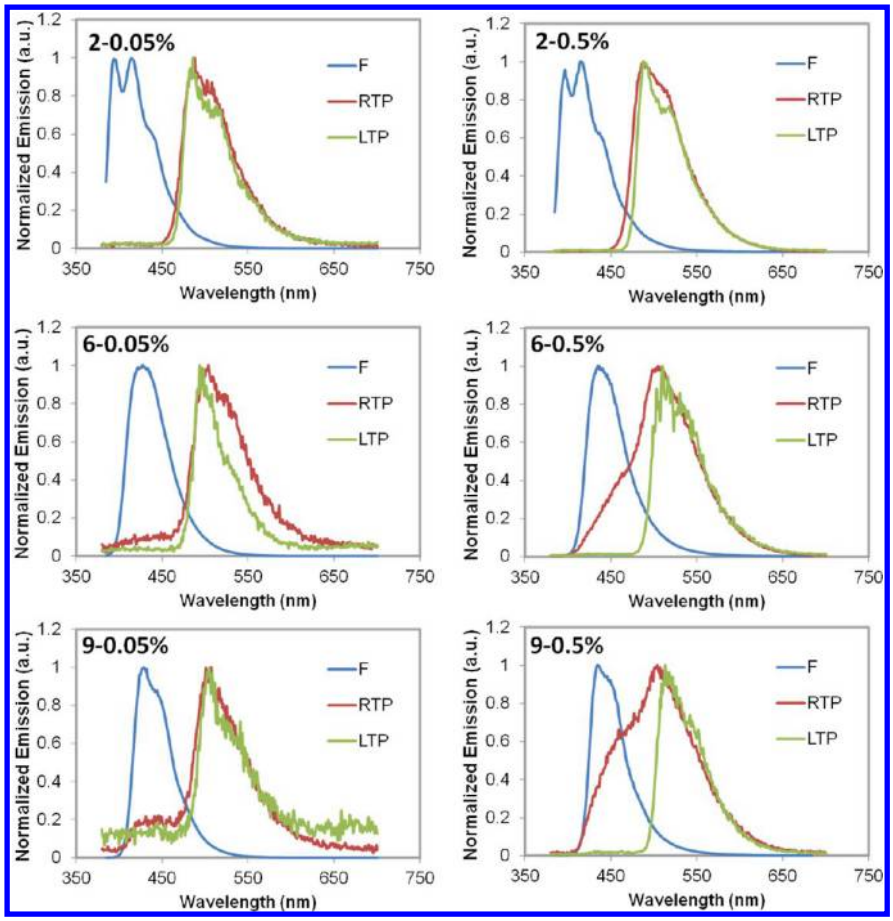

Figure 6. Normalized emission spectra for BF_2bdk complexes **2** (Ph-Ph), **6** (Ph-PhOMe), and **9** (MeOPh-PhOMe) under N_2 (left, 0.05% dye loading; right, 0.5% dye loading) at room temperature and 77 K. F, total emission spectrum under N_2 (with dominant fluoresence); RTP, room-temperature phosphorescence spectrum; LTP, low-temperature (77 K) phosphorescence spectrum. (λ_{ex} = 369 nm.)

change for **9**, PhOMe−PhOMe, from 3.71 ns at room temperature to 1.75 ns at 77 K). In fact, fluorescence lifetimes at 77 K for boron dyes at different loadings are quite close to the lifetimes at room temperature, which confirms that the lengthened lifetimes at the high loadings at room temperature are not likely to be caused by trivial effects such as reabsorption and reemission. The results suggest that even in a rigid polymer matrix such as PLA, aggregate or excimer formation is possible for smaller BF_2bdks at room temperature.

Polymer Medium Effects: Phosphorescence of BF_2bdk/PLA Blends. As described above, in PLA matrices under air, most of the complexes exhibit intense blue fluorescence except complexes **4** and **8**, which exhibit yellow and greenish-yellow emission, as shown in Figure 4. When steady-state emission spectra were acquired at 77 K for BF_2bdk/PLA blends, phosphorescence emission spectra were observed for complexes **3** (Ph-Np), **7** (Np-PhOMe), and **10** (Me-Np) (e.g., Figure 5A−C). As previously reported,[20] in the solid state, amorphous PLA serves as a rigid medium that may block thermal decay pathways and at the same time hinder quencher molecules from interacting with the dyes in the excited states.[58] Thus, in PLA matrices even room-temperature phosphorescence (RTP) is observed for BF_2bdks. Because RTP can be quenched by oxygen in ambient air, the BF_2bdk/PLA blends at two different dye loadings (0.05% and 0.5%) were also studied under a N_2 atmosphere, collecting both total emission spectra (fluorescence plus phosphorescence), RTP spectra (gated intensity), and low-temperature phosphorescence (LTP) spectra (77 K, in liquid nitrogen). Under a nitrogen atomosphere, distinct green or yellow RTP was observed for all BF_2bdks/PLA blends except for complexes **1** (Me-Ph), **4** (Ph-An), and **8** (An-PhOMe). Phosphoresence for **5** was very weak; emission maxima could be determined but lifetimes were not detectable (RT under N_2 in PLA: for 0.05% loading, 466 nm; for 0.5% loading, 487 nm). (Room- and low-temperature emission spectra for **5** in PLA are provided in the Supporting Information.)

The emission spectra of **2** (Ph-Ph), **6** (Ph-PhOMe), and **9** (PhOMe−PhOMe) (0.05% and 0.5% dye loading) are provided in Figure 6. Compared to fluorescence, the relative intensity of RTP is quite low; the total emission spectra (both fluorescence and phosphorescence under nitrogen) are nearly identical to the fluorescence spectra (under air) (Figure 4). Phosphorescence spectra, both room temperature and 77 K, were obtained by gated measurement with a delay time of 2 ms after excitation. The shoulder band observed in certain phosphorescence spectra (e.g., **2** at ∼420 nm, **6** at 427 nm, **9** at ∼430 nm), which matches the fluorescence emission, has been ascribed to delayed fluorescence caused by the thermal repopulation of the excited singlet state from the long-lived excited triplet state.[20,24] Complexes **2**, **6**, and **9** all have phenyl moieties on both sides of the diketone but are non-, mono-, and bis-methoxy-substituted, respectively. With the presence of methoxyl substituents, phosphorescence emission maxima for **6** and **9** exhibit distinct red shifts compared to **2**. Whether one or two -OMe groups are present, however, seems to have little

dx.doi.org/10.1021/ic300077g | Inorg. Chem. XXXX, XXX, XXX−XXX

Table 5. Optical Properties of BF_2bdk Complexes in PLA Matrices under Nitrogen

	0.05% (w/w) BF_2bdk/PLA				0.5% (w/w) BF_2bdk/PLA			
	λ_t,[a] nm	λ_p(RT),[b] nm	λ_p(77 K),[b] nm	τ_{pw0},[c] ms	λ_t,[a] nm	λ_p(RT),[b] nm	λ_p(77 K),[b] nm	τ_{pw0},[c] ms
2	414	488	486	513	420	488	488	581
6	422	504	494	440	439	505	510	386
9	426	501	505	402	439	504	513	214
3	439	537	533	440	454	541	542	520
7	431	538	535	463	444	541	544	424
10	427	523	522	603	434	526	527	612

[a]Total emission maxima (i.e., fluorescence peak) under N_2; excited at 369 nm. [b]Phosphorescence emission maxima under N_2; excited at 369 nm. [c]Pre-exponential weighted room-temperature phosphorescence (RTP) lifetime fit to triple-exponential decay. Excitation source: xenon flash lamp.

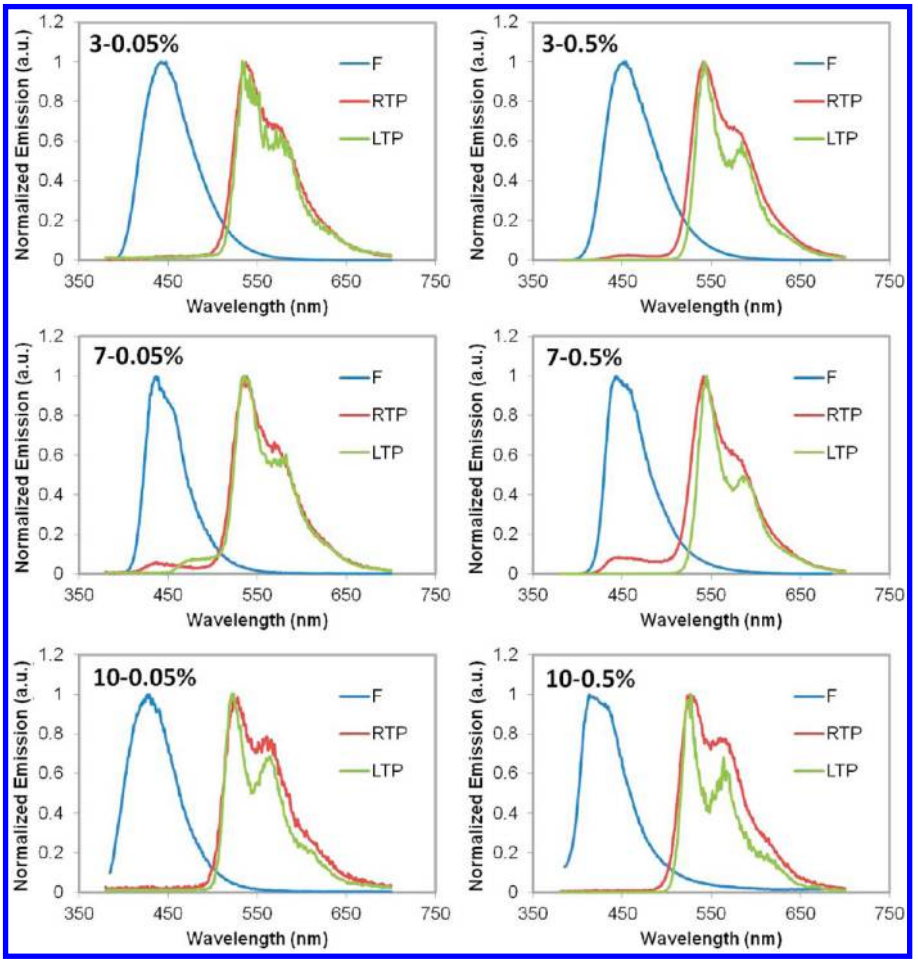

Figure 7. Normalized emission spectra for BF_2bdk complexes **3** (Ph-Np), **7** (Np-PhOMe), and **10** (Me-Np) under N_2. (Left, 0.05% dye loading; right, 0.5% dye loading) at room temperature and 77 K. F, total emission spectrum under N_2 (with dominant fluoresence); RTP, room-temperature phosphorescence spectrum under N_2; LTP, low-temperature (77K) phosphorescence spectrum. (λ_{ex} = 369 nm.)

effect on emission wavelength. Unlike the more significant red shift in fluorescence emission in going from low to high dye loading, the phosphorescence merely exhibits a slight red shift in room temperature spectra [e.g., **6**, $\Delta\lambda$ = 8 nm (430 cm^{-1}) for fluorescence (Table 3) and $\Delta\lambda$ = 1 nm (39 cm^{-1}) for phosphorescence (Table 5) from low to high dye loading]. The delayed fluorescence band intensity increases and red-shifts for the higher dye loading, consistent with previously reported dye loading effects.[24] At 77 K, where thermal back population of the singlet state is inhibited, delayed fluoresence is not evident.[20,35]

In the absence of oxygen, the RTP decay of BF_2bdk/PLA blends is complicated and can be fitted with a triple-exponential. Pre-exponential weighted lifetimes,[59] τ_{pw0}, are provided in Table 5. The phosphorescence lifetimes decrease from **2** to **6** and **9** with increasing number of methoxy groups.

Figure 7 shows the total and phosphorescence spectra of **3** (Ph-Np complex), **7** (Np-PhOMe complex), and **10** (Me-Np complex), with 0.05% and 0.5% dye loadings, respectively. Obvious phosphorescence contributions were observed in the total emission spectra for these complexes because of the relatively strong triplet emission. Similar to complexes **2**, **6**, and **9**, the phosphorescence exhibits red-shifted emission as a result of the increase of π conjugation length from complex **10** to complexes **3** and **7** (e.g., 0.05% dye loading: **10**, 523 nm; **3**, 537 nm; and **7**, 538 nm). At high dye loading, RTP lifetimes decrease for this series from **10** to **3** to **7** (612, 520, and 424 ms,

dx.doi.org/10.1021/ic300077g | Inorg. Chem. XXXX, XXX, XXX−XXX

respectively; Table 5) with increased conjugation length. Delayed fluorescence bands are also observed for complexes **3** and **7** at ~450 nm and are slightly stronger at higher loading, given a smaller singlet−triplet splitting, as previously described.[24] And again, delayed fluorescence is generally inhibited at low temperature, given decreased thermal back population.[20,35]

Computational studies were also performed for the triplet states. We modeled the phosphorescence with the following simplifying assumptions. Treating the PLA medium as a polarizable continuous medium with the same dielectric constant as dichloromethane, and optimizing the lowest triplet with B3LYP/6-31G(d) to obtain $E(T_1)$, we can approximate the energy of the phosphorescence as either (a) the energy difference between that triplet energy $E(T_1)$ and the $E(S_0)$ energy obtained with B3LYP/6-31G(d) at that same geometry or (b) the transition energy for the singlet−triplet excitation as computed by TD/6-311+G(d) at the B3LYP/6-31G(d) optimized T_1 geometry. Table 6 shows values of estimates of

Table 6. Phosphorescence Emission Maxima and Computational Estimates of the Singlet−Triplet Gaps

	emission maxima, nm		wavelengths, nm	
	0.05% in PLA/N_2	0.5% in PLA/N_2	from TD S−T absorption[a]	from B3LYP S−T energy gap[b]
1			540	501
2	486	488	564	554
3	533	542	701	621
4			1105	899
5	466	478	549	510
6	494	505	590	547
7	535	544	691	611
8			1095	886
9	505	504	590	548
10	522	527	697	616

[a]Singlet−triplet excitation energy estimated by TD-B3LYP/6-311+G(d), at the UB3LYP/6-31G(d) optimized T_1 geometry. [b]Direct differences of B3LYP/6-31G(d) for singlet and UB3LYP/6-31G(d) for triplet, all at the UB3LYP/6-31G(d) optimized T_1 geometry.

both types. Linear regression shows a correlation statistic R^2 = 0.89 between observed phosphorescence wavelengths and values computed by direct difference of B3LYP/6-31G(d) values, and R^2 = 0.92 between observed values and estimates from TD/6-311+G(d)//B3LYP/6-31G(d) calculations. Though the linearity as measured by the R^2 statistic is slightly better for the TD calculations than for direct energy differences, the TD estimates are more seriously shifted to the red. The very red results for complexes **4** and **8** suggest that their phosphorescence may lie outside the region monitored experimentally with the present instrumentation and hence would explain why phosphorescence was not observed for these anthryl derivatives.

In summary, when the dye complexes were excited from the ground state to a higher vibrational level of S_1 (or S_2), the majority of the molecules readily relax (10^{-12} s) to the lowest vibrational level, S_1, through internal conversion. From the S_1 state, excited molecules may decay radiatively in several nanoseconds and exhibit fluorescence. They can also undergo a spin conversion to the triplet state by intersystem crossing and exhibit phosphorescence. Although this and the reverse processes are spin-forbidden, under certain conditions, back population can occur by thermal excitation of the singlet state from the triplet state if the thermal energy kT is comparable to the S_1-T_1 energy gap.[60] Therefore, the energy gap between S_1 and T_1 has an important influence on this reverse conversion. Given the molecular structure of these complexes, we may draw a preliminary conclusion. Complexes with greater π conjugation length (e.g., **3** and **7** versus **10**) and donor strength (e.g., **6** and **9** versus **2**), are more inclined to undergo reverse intersystem crossing, perhaps because a lower energy S_1 level decreases the S_1-T_1 energy gap. For higher dye loading, dye−dye distances are shorter, aggregates may form, and the medium is more polar. Under these circumstances, singlet-state energy also decreases while phosphoresence energy is little affected, facilitating intersystem crossing.

CONCLUSION

In summary, we have synthesized a class of aromatic hydrocarbon-substituted difluoroboron diketonate complexes (BF_2bdks) ranging from methyl, phenyl, methoxyphenyl, naphthyl, to anthryl groups on either side of the diketonate ligands. The optical properties of these boron complexes were studied in CH_2Cl_2 and in the solid-state solvent PLA. In CH_2Cl_2, the absorption, fluorescence emission, and fluorescence lifetimes were investigated for all of the BF_2bdks. It was found that almost all complexes exhibit intense fluorescence emission (ϕ_F 0.26−1) except for one molecule, which has phenyl and methyl groups on the BF_2bdk (**1**). While one might think that simply extending the conjugation would lead to red-shifted dyes, there appear to be two or more factors at play, and properties in PLA environments are different than in solution. The emission colors of the series of boron dyes are correlated not only to the length of their π conjugation but also to the tendency for intramolecular charge transfer (ICT) in solution; larger π conjugation and stronger ICT result in more red-shifted emission. In a lifetime study, we discovered that the extent of the ICT processes for these molecules are determined by the electron-donating ability of the arene groups on the two sides of the diketonate complexes. A bigger difference in electron-donating ability on the two sides correlates with stronger ICT and longer fluorescence lifetime, which is predicted by modeling and calculations. The optical properties of these boron dyes were then investigated in PLA substrates at two different dye loadings, 0.05% and 0.5%, at both room temperature and 77 K. Most of the boron complexes exhibit slightly blue-shifted emission and reduced fluorescence lifetimes in PLA at lower dye loadings, suggesting the hindrance of ICT processes by the polymer medium. At higher dye loadings, however, both spectra and lifetimes representative of aggregate or excimeric species were observed, which is consistent with the previous report[24] and has been ascribed to dye−dye interactions in close proximity. These interactions were reduced at 77 K, possibly due to the rigidity of the medium, which can limit the configurations required for excimeric species. Delayed emission, namely, phosphorescence and delayed fluorescence, are also present for many dyes in PLA environments under nitrogen. Studying the emission properties of these model compounds may inform the rational design of BF_2bdks for practical applications in imaging and sensing.

ASSOCIATED CONTENT

Supporting Information

Seven tables listing B3LYP/6-31+G(d) and B3LYP/6-31G(d)/PCM optimized ground-state structures and Gaussian log files

dx.doi.org/10.1021/ic300077g | Inorg. Chem. XXXX, XXX, XXX−XXX

for TD-DFT calculations, MO diagrams for accessible optical electronic transitions, graphs of computed spectra, results for triplets B3LYP/6-31G(d) in dichloromethane, and singlet−triplet transitions B3LYP/6-311+G(d) in dichloromethane; five figures showing excitation spectra for complexes **4** and **8** in CH_2Cl_2 solution and PLA and room- and low-temperature emission spectra for **5** in PLA; and additional text giving full computational details. This material is available free of charge via the Internet at http://pubs.acs.org.

AUTHOR INFORMATION

Corresponding Author

*E-mail: fraser@virginia.edu.

Present Addresses

†G.Z.: CAS Key Laboratory of Soft Matter Chemistry, Department of Polymer Science and Engineering, University of Science and Technology of China, Hefei, Anhui, 230026, China. E-mail: gzhang@ustc.edu.cn.

‡R.E.E.: Department of Physics, Harvard University, Cambridge, Massachusetts 02138, United States. E-mail: ruffinevans@fas.harvard.edu.

Notes

The authors declare no competing financial interest.

ACKNOWLEDGMENTS

We thank the National Science Foundation (CHE 0718879, CHE 1213915) for support for this research, and the Goldwater Scholarship Foundation for a scholarship to R.E.E. This work was also supported in part by the National Cancer Institute of the National Institutes of Health (R01 CA167250), and the UVA Cancer Center through the Farrow Fellowship Fund and the NIH NCI Cancer Center Support Grant (P30 CA44579). We also thank Nguyen D. Nguyen and Alan D. Chien for their assistance.

REFERENCES

(1) Jäkle, F. *J. Inorg. Organomet. Polym. Mater.* **2005**, *15*, 293.
(2) Cheng, F.; Jäkle, F. *Polym. Chem.* **2011**, *2*, 2122.
(3) Nagai, A.; Chujo, Y. *Chem. Lett.* **2010**, *39*, 430.
(4) Jäkle, F. *Chem. Rev.* **2010**, *110*, 3985.
(5) Ono, K.; Yoshikawa, K.; Tsuji, Y.; Yamaguchi, H.; Uozumi, R.; Tomura, M.; Taga, K.; Saito, K. *Tetrahedron* **2007**, *63*, 9354.
(6) Chow, Y. L.; Cheng, X. *Can. J. Chem.* **1991**, *69*, 1331; 1575.
(7) Chow, Y. L.; Ouyang, X. *Can. J. Chem.* **1991**, *69*, 423.
(8) Chow, Y. L.; Wang, S. S. *Can. J. Chem.* **1993**, *71*, 846.
(9) Chow, Y. L.; Cheng, X.; Johansson, C. I. *J. Photochem. Photobiol. A: Chem.* **1991**, *57*, 247.
(10) Ilge, H. D.; Birckener, E.; Fassler, D.; Kozmenko, M. V.; Kanzmin, M. G.; Hortman, H. *J. Photochem.* **1986**, *32*, 177.
(11) Schade, W.; Ilge, H. D.; Hartman, H. *J. Prakt. Chem.* **1986**, *328*, 941.
(12) Padilha, L. A.; Webster, S.; Przhonska, O. V.; Hu, H.; Peceli, D.; Ensley, T. R.; Bondar, M. V.; Gerasov, A. O.; Kovtun, Y. P.; Shandura, M. P.; Kachkovski, A. D.; Hagan, D. J.; Stryland, E. W. V. *J. Phys. Chem. A.* **2010**, *114*, 6493.
(13) Cogné-Laage, E.; Allemand, J.-F.; Ruel, O.; Baudin, J.-B.; Croquette, V.; Blanchard-Desce, M.; Jullien, L. *Chem.—Eur. J.* **2004**, *10*, 1445.
(14) Nagai, A.; Kokado, K.; Nagata, Y.; Chujo, Y. *Macromolecules* **2008**, *41*, 8295.
(15) Nagata, Y.; Otaka, H.; Chujo, Y. *Macromolecules* **2008**, *41*, 737.
(16) (a) Qin, Y.; Kiburu, I.; Shah, S.; Jäkle, F. *Macromolecules* **2006**, *39*, 9041. (b) Jäkle, F. *Coord. Chem. Rev.* **2006**, *250*, 1107.
(17) Ono, K.; Hashizume, J.; Yamaguchi, H.; Tomura, M.; Nishida, J.-i.; Yamashita, Y. *Org. Lett.* **2009**, *11*, 4326.
(18) Poon, C.; Lam, W. H.; Wong, H.; Yam, V. W. *J. Am. Chem. Soc.* **2010**, *132*, 13992.
(19) Ran, C.; Xu, X.; Raymond, S. B.; Ferrara, B. J.; Neal, K.; Bacskai, B. J.; Medarova, Z.; Moore, A. *J. Am. Chem. Soc.* **2009**, *131*, 15257.
(20) Zhang, G.; Chen, J.; Payne, S. J.; Kooi, S. E.; Demas, J. N.; Fraser, C. L. *J. Am. Chem. Soc.* **2007**, *129*, 8942.
(21) Zhang, G.; Lu, J.; Sabat, M.; Fraser, C. L. *J. Am. Chem. Soc.* **2010**, *132*, 2160.
(22) Huang, M.; Lou, Y.; Xie, J.; Ma, W.; Lu, Y.; Yen, P.; Zhu, B.; Newmark, H.; Ho, C. *Carcinogenesis* **1998**, *19*, 1697.
(23) Chatelain, E.; Gabard, B. *Photochem. Photobiol.* **2001**, *74*, 401.
(24) Zhang, G.; Kooi, S. E.; Demas, J. N.; Fraser, C. L. *Adv. Mater.* **2008**, *20*, 2099.
(25) Zhang, G.; Palmer, G. M.; Dewhirst, M. W.; Fraser, C. L. *Nat. Mater.* **2009**, *8*, 747.
(26) Palmer, G. M.; Fontanella, A. N.; Zhang, G.; Hanna, G.; Fraser, C. L.; Dewhirst, M. W. *J. Biomed. Opt.* **2010**, *15*, No. 066021.
(27) Pfister, A.; Zhang, G.; Zareno, J.; Horwitz, A. F.; Fraser, C. L. *ACS Nano* **2008**, *2*, 1252.
(28) Contreras, J.; Xie, J.; Chen, Y. J.; Pei, H.; Zhang, G.; Fraser, C. L.; Hamm-Alvarez, S. *ACS Nano* **2010**, *4*, 2735.
(29) Rubart, M. *Circ. Res.* **2004**, *95*, 1154.
(30) Mirochnik, A. G.; Bukvetskii, B. V.; Fedorenko, E. V.; Karasev, V. E. *Russ. Chem. Bull.* **2004**, *53*, 291.
(31) Mirochnik, A. G.; Gukhman, E. V.; Karasev, V. E.; Zhikhareva, P. A. *Russ. Chem. Bull.* **2000**, *49*, 1024.
(32) Mayoral, M. J.; Cornago, P.; Claramunt, R. M.; Cano, M. *Dalton Trans.* **2010**, *40*, 377.
(33) Nagai, A.; Kokado, K.; Nagata, Y.; Arita, M.; Chujo, Y. *J. Org. Chem.* **2008**, *73*, 8605.
(34) Domercq, B.; Grasso, C.; Maldonado, J. L.; Halik, M.; Stephen, B.; Marder, S. R.; Kippelen, B. *J. Phys. Chem. B* **2004**, *108*, 8647.
(35) Payne, S. J.; Zhang, G.; Demas, J. N.; Fraser, C. L.; DeGraff, B. A. *Appl. Spectrosc.* **2011**, *65*, 1321.
(36) Zhang, G.; Fiore, G. L.; St. Clair, T. L.; Fraser, C. L. *Macromolecules* **2009**, *42*, 3162.
(37) Loudet, A.; Burgess, K. *Chem. Rev.* **2007**, *107*, 4891.
(38) Ulrich, G.; Ziessel, R.; Harriman, A. *Angew. Chem., Int. Ed.* **2008**, *48*, 1184.
(39) Liu, T.; Chien, A. D.; Lu, J.; Zhang, G.; Fraser, C. L. *J. Mater. Chem.* **2011**, *21*, 8401.
(40) Demas, J. N.; Crosby, G. A. *J. Phys. Chem.* **1971**, *75*, 991 (section II.C.2, eq 16).
(41) Dawson, W. R.; Windsor, M. W. *J. Phys. Chem.* **1968**, *72*, 3251.
(42) Frisch, M. J.; Trucks, G. W.; Schlegel, H. B.; Scuseria, G. E.; Robb, M. A.; Cheeseman, J. R.; Scalmani, G.; Barone, V.; Mennucci, B.; Petersson, G. A.; Nakatsuji, H.; Caricato, M.; Li, X.; Hratchian, H. P.; Izmaylov, A. F.; Bloino, J.; Zheng, G.; Sonnenberg, J. L.; Hada, M.; Ehara, M.; Toyota, K.; Fukuda, R.; Hasegawa, J.; Ishida, M.; Nakajima, T.; Honda, Y.; Kitao, O.; Nakai, H.; Vreven, T.; Montgomery, Jr., J. A.; Peralta, J. E.; Ogliaro, F.; Bearpark, M.; Heyd, J. J.; Brothers, E.; Kudin, K. N.; Staroverov, V. N.; Kobayashi, R.; Normand, J.; Raghavachari, K.; Rendell, A.; Burant, J. C.; Iyengar, S. S.; Tomasi, J.; Cossi, M.; Rega, N.; Millam, J. M.; Klene, M.; Knox, J. E.; Cross, J. B.; Bakken, V.; Adamo, C.; Jaramillo, J.; Gomperts, R.; Stratmann, R. E.; Yazyev, O.; Austin, A. J.; Cammi, R.; Pomelli, C.; Ochterski, J. W.; Martin, R. L.; Morokuma, K.; Zakrzewski, V. G.; Voth, G. A.; Salvador, P.; Dannenberg, J. J.; Dapprich, S.; Daniels, A. D.; Farkas, Ö.; Foresman, J. B.; Ortiz, J. V.; Cioslowski, J.; Fox, D. J. *Gaussian 09, Revision A.02*; Gaussian, Inc., Wallingford, CT, 2009.
(43) Becke, A. D. *J. Chem. Phys.* **1993**, *98*, 5648.
(44) Lee, C.; Yang, W.; Parr, R. G. *Phys. Rev. B* **1988**, *37*, 785.
(45) Macedo, F. P.; Gwengo, C.; Lindeman, S. V.; Smith, M. D.; Gardinier, J. R. *Eur. J. Inorg. Chem.* **2008**, 3200.
(46) Ono, K.; Yamaguchi, H.; Taga, K.; Saito, K.; Nishida, J.-i.; Yamashita, Y. *Org. Lett.* **2008**, *11*, 149.
(47) Truong, T.-T.; Brenner, V.; Ledoux, G.; Tran-Thi, T.-H. *Photochem. Photobiol. Sci.* **2006**, *5*, 686.

(48) Yoshihiro, Y.; Yoshio, M.; Takanori, O.; Tateaki, W.; Zen-ichi, Y. *J. Am. Chem. Soc.* **2008**, *130*, 13867.
(49) Zhang, G.; Kim, S. H.; Evans, R. E.; Kim, B. H.; Demas, J. N.; Fraser, C. L. *J. Fluoresc.* **2009**, *19*, 881.
(50) Dreuw, A.; Weisman, J. L.; Head-Gordon, M. *J. Chem. Phys.* **2003**, *119*, 2943.
(51) Cohen, A. J.; Mori-Sánchez, P.; Yang, W. *Science* **2008**, *321*, 792.
(52) Dreuw, A.; Head-Gordon, M. *J. Am. Chem. Soc.* **2004**, *126*, 4007.
(53) Chai, J.; Head-Gordon, M. *J. Chem. Phys.* **2008**, *128*, 084106.
(54) Dechy-Cabaret, O.; Martin-Vaca, B.; Bourissou, D. *Chem. Rev.* **2004**, *104*, 6147.
(55) Peinado, C.; Salvador, E. F.; Catalina, F.; Lozano, A. E. *Polymer* **2001**, *42*, 2815.
(56) Grabowski, Z. R.; Rotkiewicz, K.; Rettig, W. *Chem. Rev.* **2003**, *103*, 3899.
(57) Sun, X.; Zhang, X.; Li, X.; Liu, S.; Zhang, G. *J. Mater. Chem.* **2012**, *22*, 17332.
(58) Mitchell, C. A.; Gurney, R. W.; Jang, S.-H.; Kahr, B. *J. Am. Chem. Soc.* **1998**, *120*, 9726.
(59) Carraway, E. R.; Demas, J. N.; DeGraff, B. A. *Anal. Chem.* **1991**, *63*, 332.
(60) Fister, J. C., III; Rank, D.; Harris, J. M. *Anal. Chem.* **1995**, *67*, 4269.

dx.doi.org/10.1021/ic300077g | *Inorg. Chem.* XXXX, XXX, XXX−XXX